Temperature dependence of the magnetic-flux penetration into disk-shaped $YBa_2Cu_3O_{7-\delta}$ thin films

H. Darhmaoui and J. Jung
Department of Physics, University of Alberta, Edmonton, Alberta, Canada T6G 2J1

J. Talvacchio
Westinghouse Science and Technology Center, Pittsburgh, Pennsylvania 15235

M. A-K. Mohamed*
Department of Physics, University of Lethbridge, Lethbridge, Alberta, Canada T1K 3M4

L. Friedrich
Department of Electrical Engineering, University of Alberta, Edmonton, Alberta, Canada T6G 2G7
(Received 5 July 1995; revised manuscript received 21 December 1995)

Temperature dependence of the penetration of magnetic flux into $YBa_2Cu_3O_{7-\delta}$ disk-shaped thin films was investigated at low magnetic fields. We studied the conditions characteristic of complete and incomplete flux-penetration states. The experimental procedure involved the measurements of the profiles of trapped magnetic flux as a function of temperature and the decays of trapped flux at various points across the disk. We determined temperatures and magnetic fields at which the crossover between incomplete and complete flux penetration occurs. This crossover is governed by the temperature dependence of the critical current density. The distributions of the critical currents across the disk in the complete flux-penetration state were found to be temperature independent. No evidence for the Bean-Livingston surface barriers has been found. [S0163-1829(96)03518-7]

I. INTRODUCTION

Studies of magnetic-flux penetration into superconducting thin films have been recognized as those which provide important information on critical currents, on distribution of shielding currents and weak links, on demagnetization effects, and on complete and partial flux penetration states. Results obtained on thin films of circular geometry (which ensures homogeneous penetration of flux) seem to be particularly useful due to the need for verification of the conventional critical state model. Penetration of magnetic flux into disk-shaped thin films of $YBa_2Cu_3O_{7-\delta}$ (YBCO) has been studied with the magneto-optical Faraday rotation method.[1,2] Calculation of the distribution of both the axial and radial components of the magnetic field across a thin circular film has been performed by Theuss, Forkl, and Kronmüller[3] for film thicknesses smaller than the London penetration depth. Good agreement was obtained between the calculated distribution of the axial component of the field and the experimental data (Ref. 2). However, the authors admitted that the magneto-optical measurements do not provide an evidence of a complete flux penetration (which is, on the other hand, given by the saturation of dc magnetization in increasing applied magnetic field) due to insensitivity of a central fringe area, of width about 20% of the disk's radius, to the penetrating magnetic field. The available experimental data are insufficient to explain deviation of the magnetic-flux distribution from that predicted by the conventional critical state model. This applies both to the distribution of the radial component of the magnetic induction B_r, for which there are recorded no experimental data, and to the distribution of the axial component B_z, with missing temperature and magnetic-field dependence of the complete flux-penetration states. This information is crucial for the analysis of the critical state model (and its applicability to thin-film superconductors) which has been proposed by Theuss, Forkl, and Kronmüller,[3] Däumling and Larbalestier,[4] Conner and Malozemoff,[5] and Brandt.[6] The leading conclusion of this analysis is that in the case of thin-film circular samples, the critical state model requires modification by taking into account dominating influence of the gradient of the field component $\partial B_r/\partial z$ on the critical current density $J_c=(1/\mu_0)(\partial B_r/\partial z-\partial B_z/\partial r)$, where $\partial B_r/\partial z$ is much larger than $\partial B_z/\partial r$. Therefore, the critical state in the disk occurs rather through the thickness d, and not the radius r. Theuss, Forkl, and Kronmüller[3] showed that in the absence of the experimental data for the radial component $B_r(r)$, one could calculate it using experimental results for $B_z(r)$. Their computation consists of the following steps:

(a) Fitting of the current distribution $I(r)$ to the Biot-Savart law, so it could reproduce the experimental distribution of $B_z(r)$;
(b) Calculation of the radial component $B_r(r)$ from the Biot-Savart law using the current distribution $I(r)$;
(c) Estimation of $\partial B_r/\partial z$ by taking $\partial B_r/\partial z \approx 2B_r(d/2)/d$ [where $B_r(d/2)$ is the field on the surface] under the assumption that $B_r(z)$ vary smoothly through the film thickness d.

This procedure was used to compare the $\partial B_z/\partial r \approx B_z(a)/a$ term (where a is the radius of the thin-film disk) with that for

 © 1996 The American Physical Society

$\partial B_r/\partial z \approx 2B_r(d/2)/d$ in the formula for the current density. Comparison of the experimental $B_z(r)$ with the calculated $B_r(r)$ shows that at low magnetic inductions $B_r(d/2)$ on the disk's surface and $B_z(a)$ on the disk's surface and at the disk's edge are of the same order of magnitude. This implies that $\partial B_r/\partial z$ is greater than $\partial B_z/\partial r$ approximately by a factor of a/d.

Briefly, the analysis of Theuss, Forkl, and Kronmüller[3] suggests that the knowledge of an experimental distribution $B_z(r)$ across a disk-shaped thin film is essential for an estimation of the distribution of the current $I(r)$ and its dependence on an external magnetic field, which can be used further to calculate magnetic stray field effects. It is therefore worthwhile to expand the investigations of $B_z(r)$ by performing the following experiments:

(a) Measurements of the temperature and magnetic-field dependence of an incomplete-complete flux-penetration states;
(b) Measurements of the time dependence of the $B_z(r)$ profiles for an incomplete and complete flux-penetration states, and
(c) Measurements of the magnitude of the applied magnetic field required for a full flux penetration.

We have attempted to make the above measurements using a Hall-probe scanning system. A Hall-probe scanning system has been used by us since 1988 for studies of magnetic-flux distributions and persistent currents in YBCO ceramic disks and rings (Ref. 7). This system provides better accuracy regarding the measurement of a magnitude of the magnetic field than the corresponding magneto-optical Faraday effect method. It is also free of the unwanted change in sensitivity, shown by a magneto-optical method,[3] during the measurement of the field distribution between the edge and the center of the disk-shaped sample. A Hall-probe scanning system also allows to measure, with high accuracy, the time-dependent changes in $B_z(r)$ at any point along the disk's diameter.

The measurements of the flux penetration condition were made using the distribution of the trapped field rather than the shielding field. The advantage of that is much more precise determination of the transition between the partial and complete penetration of magnetic flux. The results were compared with the predictions of the existing critical state models[3–6] and with the measurements of the flux and current distributions in a square-shaped thin film of YBCO by Xing *et al.*[8] and Grant *et al.*[9]

II. EXPERIMENTAL PROCEDURE

A. Sample's preparation and characterization

Two thin-film YBCO disks, having diameter of 15 mm and thickness of 5000 Å (disk No. 1) and 2000 Å (disk No. 2), were sputter-deposited on (100)-oriented $LaAlO_3$ substrates using off-axis dc magnetron sputtering from a stoichiometric YBCO target.[10] The films were c-axis oriented, with the c axis perpendicular to the disk's plane. The resistive measurement of superconducting transition gave T_c ($R=0$) of 90.3 K for disk No. 1, and of 89.2 K for disk No. 2. The measurement of the real part of ac susceptibility $\chi(T)$ with $f=3.22$ kHz and $H_{\rm rms}=1.8$ G, revealed $T_c=87$ K, for disk No. 1 and 86 K for disk No. 2, and the width of the superconducting transition $\Delta T \approx 1.5$ K in both cases. The imaginary part of ac susceptibility $\chi'(T)$ shows a sharp peak at 86 K for disk No. 1 and at 85 K for disk No. 2.

B. Magnetic-flux-penetration measurement procedure

Magnetic-flux penetration was inferred from the measurements of the trapped magnetic-flux density across the disk as a function of temperature and applied magnetic field. The measurements were done with a scanning Hall-probe system. A Hall probe of the sensitive area of 0.4 mm^2 and sensitivity of 20–30 mG was used to record distributions of magnetic field at a distance of 1.6 mm above the disk. Time dependence of the magnetic-flux density was measured with a Hall probe at various points along the disk's diameter for a time range of up to 10^4 sec. The details of the experimental setup, that was used in these studies, are reported in Ref. 11. The measurement of magnetic-flux penetration was based on the following procedure. After zero-field cooling (ZFC) the disk down to various temperatures below T_c, the external magnetic field was applied in a direction perpendicular to the disk's plane and parallel to the film's c axis (the external magnetic field over a range 0–750 G was generated by nonsuperconducting solenoid). This was followed by the measurement of the profile of the axial component of the shielding field (which is the difference between the applied field and the field measured by the probe) and that produced by the trapped field when the external magnetic field was reduced to zero. The information on an incomplete and complete flux penetration was obtained by

(a) plotting the magnitude of the trapped field in the disk's center versus temperature for a constant applied magnetic field, and by
(b) plotting the decay rates of the trapped field (recorded at various points along the disk's diameter) versus distance from the disk's center for fixed temperatures and applied magnetic field.

C. Critical current measurement procedure

The temperature dependence of the critical current was inferred from the temperature dependence of the magnetic field generated at the center of a ring by the persistent circulating current at the critical level. The ring of the outer diameter of 8.5 mm and the inner diameter of 5 mm was etched from disk No. 1 using the photolithography technique. The persistent current was induced in the zero-field-cooled ring by applying and subsequently switching off the external magnetic field. The profile of the magnetic field produced by the current was measured with a scanning Hall probe. The profile due to the current has a single maximum at the ring's center, which can be distinguished from that due to the magnetic vortices trapped in the ring's bulk which exhibits two maxima above the ring's bulk and a minimum in the ring's center. The magnitude of the critical current is proportional to the saturation value of the magnetic induction in the ring's center according to the Biot-Savart law (this can be achieved by increasing the external magnetic field). The magnetic-field dependence of the critical current was measured in the field-cooled ring. After field cooling down to a

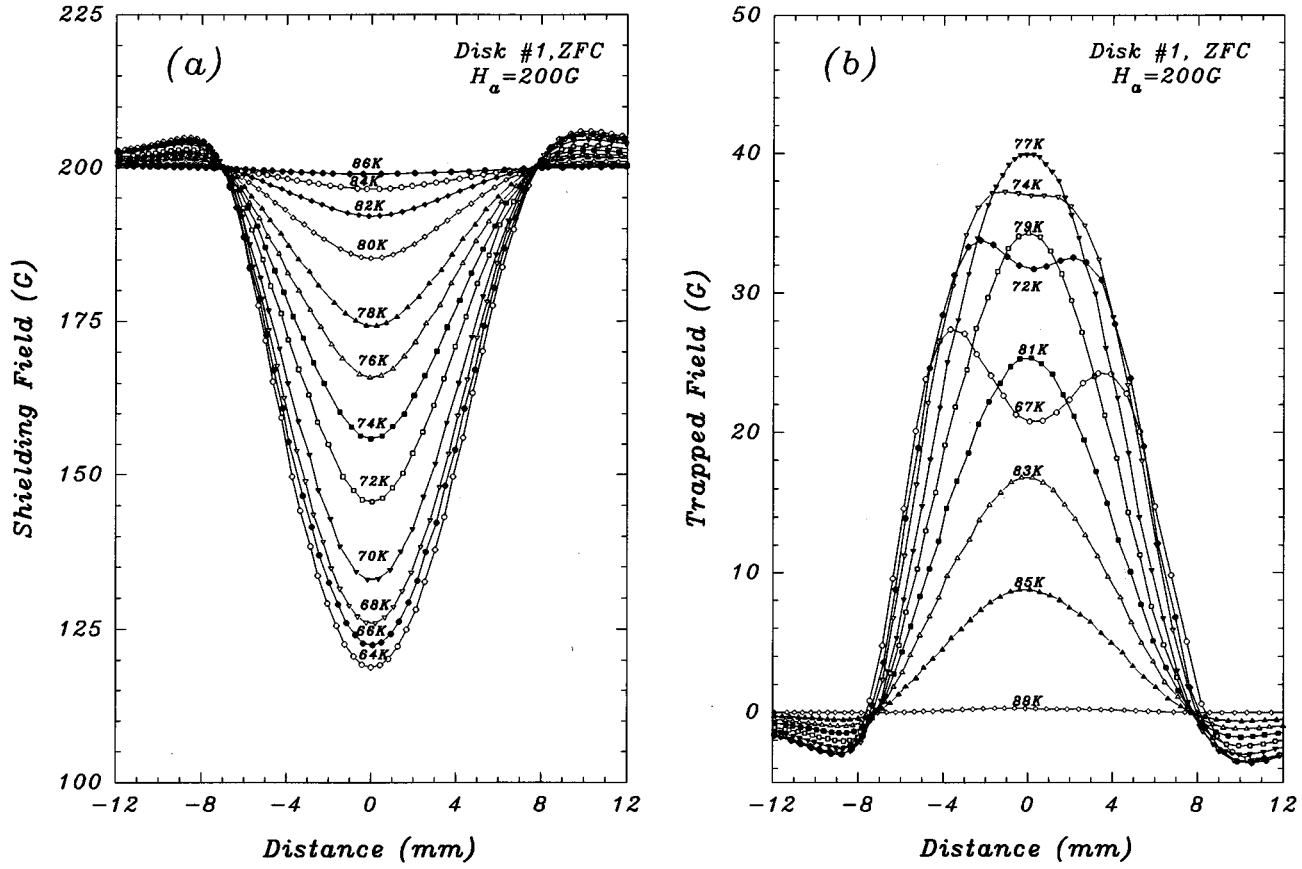

FIG. 1. (a) The profiles of the magnetic field shielded by the zero-field-cooled disk No. 1 at various temperatures between 60 and 90 K in the presence of an external field of 200 G. The profiles are measured by a scanning Hall probe at a distance of 1.6 mm from the sample. Distances +7.5 mm and −7.5 mm mark the disk edges. (b) The profiles of the magnetic field trapped in the zero-field cooled disk No. 1 at various temperatures between 60 and 90 K after the external field of 200 G was switched off. Note that above 77 K the complete flux-penetration state was reached.

certain temperature, the additional external magnetic field was applied. This was followed by the measurements of the axial component of the persistent current's self-field, when the additional external field was reduced to zero. In this case, the self-field of the current was superposed on the Meissner field. Similarly to the ZFC case, the value of the critical current was determined from the saturation value of the axial component of the current's self-field in the ring's center (see Ref. 11 for details of this procedure).

III. EXPERIMENTAL RESULTS

The profiles of the magnetic field shielded by disk No. 1 when an external magnetic field of 200 G was applied to the zero-field-cooled (ZFC) sample are plotted in Fig. 1(a) for various temperatures between 60 and 86 K. These distributions do not indicate which temperature corresponds to a complete penetration of the magnetic flux into the disk. This information is provided by the profiles of the magnetic field trapped in the disk at various temperatures when the external field of 200 G was reduced to zero [Fig. 1(b)]. The crossover between partial and complete flux penetration can be seen even clearer in Fig. 2 where the magnetic field trapped in the disk's center is plotted versus temperature for constant applied magnetic fields of 40, 80, 123, and 200 G. The maximum in the trapped field (and the inflection point on the shielding field versus temperature curve) indicate the crossover temperature. The magnitude of the trapped field at the maximum decreases linearly with increasing crossover temperature [Fig. 3(a)]. This could also be seen in Fig. 2(d). The maximum trapped field is also proportional to the minimum magnitude of the applied field required for a complete flux penetration [Fig. 3(b)]. The temperature dependence of the maximum field trapped in the disk and that of the magnetic field generated by the critical persistent current circulating in the ring coincide (Fig. 4). Figures 5(a) and 5(b) show the distributions of the trapped magnetic flux measured across disk No. 1 at 79 K (corresponding to the complete flux-penetration state after a field of 200 G was applied to the zero-field-cooled sample) and at 67 K (corresponding to the incomplete flux penetration). They are plotted together with the distribution of the normalized decay rates $S=(1/B_0)dB/d\ln t$ for the motion of the trapped flux (S was measured over a time range $1–10^4$ sec). The complete flux-penetration condition is characterized by the normalized decay rates which do not vary much ($0.012<S<0.015$) across the disk. For the incomplete flux penetration S has a minimum (at $S=0.0045$) at the disk's center and a maximum (at $S=0.012$) at the disk's edge. The magnetic field trapped in the disk's center when a field of 200 G was applied to the

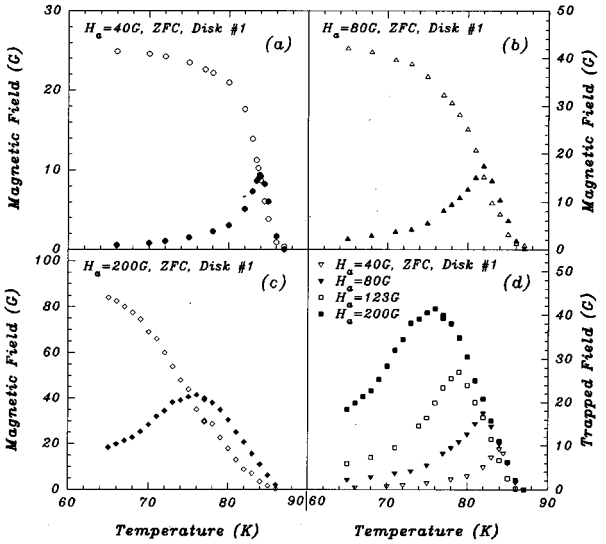

FIG. 2. Open symbols mark temperature dependence of the magnetic field shielded in the center of the zero-field-cooled disk No. 1 in the presence of external fields of 40 G (a), 80 G (b), and 200 G (c). Solid symbols mark temperature dependence of the magnetic field trapped in the center of the disk after the applied field was reduced to zero. The maximum trapped field indicates the crossover between the partial and complete flux-penetration states. Note that this maximum coincides with the inflection point on the shielding field versus temperature curve. (d) Temperature dependence of the field trapped in disk No. 1, plotted for various applied fields between 40 and 200 G. The complete flux-penetration state is common for all trapped fields at temperatures higher than that corresponding to the maximum trapped field. Discrepancies observed for various applied fields are caused by the time decay of the trapped field.

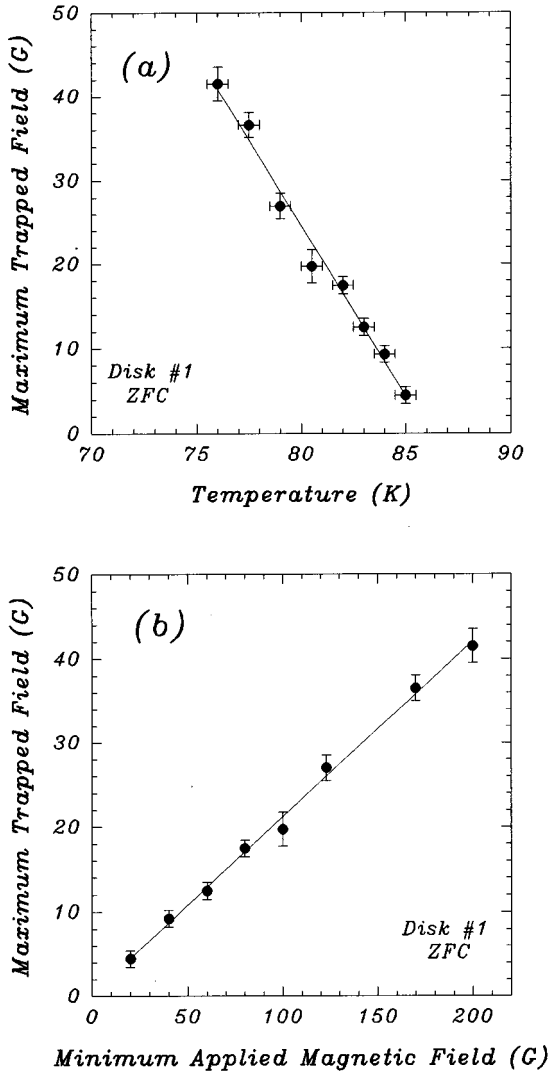

FIG. 3. (a) Temperature dependence of the maximum magnetic field which can be trapped in the center of the zero-field-cooled disk No. 1. (b) Dependence of the maximum trapped field on the minimum magnitude of the external magnetic field required for a complete flux penetration.

zero-field-cooled sample is plotted with the corresponding normalized decay rates versus temperature (over a range of 65–85 K) in Fig. 5(c). The decay rates are independent of temperature at temperatures corresponding to the complete (with average $S=0.015$) and incomplete (with average $S=0.0055$) flux penetration states. The decay rates in the complete flux-penetration regime are approximately two times the value observed for the incomplete flux penetration at the same temperature range [Figs. 5(c) and 5(d)]. The normalized decay rates S were measured at the disk's center for a complete flux-penetration state (after applying a saturating magnetic field of 750 G to the zero-field-cooled sample) over a range of temperatures between 60 and 85 K. The decay rates are logarithmic in time up to a maximum waiting time of 10^4 sec. The decay rates S are plotted, together with the corresponding flux-pinning energy $E_0=kT/S$ and the trapped field, versus temperature in Fig. 5(d). The transition between complete and incomplete flux penetration can be seen also in disk No. 2, however, the applied magnetic field required to reach the full flux-penetration state at fixed temperature, is about a factor of 4 smaller than the corresponding applied field for disk No. 1. Figure 6(a) shows different stages of flux penetration into disk No. 2 at 30 K, after an increasing external magnetic field (up to 750 G) was applied to the zero-field-cooled sample. The distributions of the trapped magnetic field, in a complete flux-penetration state are presented in Fig. 6(b) for temperatures between 30 and 85 K. The field trapped in the disk's center decreases linearly with increasing temperature [Fig. 6(c)]. For ring No. 1, the magnetic field trapped in the center of the zero-field-cooled ring, when a field of 200 G was applied to it, is plotted together with the corresponding normalized decay rates versus temperature (over a range of 50–85 K) in Fig. 7(a). The decay rates are independent of temperature at temperatures above 64 K, corresponding to the full critical state (with average $S=0.0145$), and at temperatures below 63 K, corresponding to the partial critical state (with average $S=0.0025$). The distributions of the trapped magnetic field, in a full and partial critical state, are presented in Fig. 7(b), for temperatures between 50 and 90 K.

IV. DISCUSSION

The profiles of the magnetic induction measured across the thin-film disk, when an external field is shielded by it

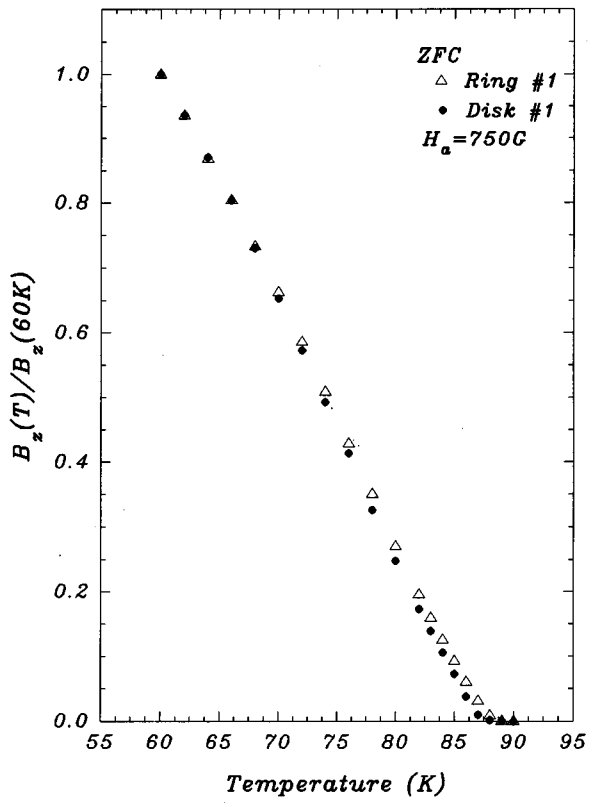

FIG. 4. Temperature dependence of the maximum field trapped in the zero-field-cooled disk No. 1 (solid symbols) and that of the magnetic field generated by the critical persistent current circulating in the zero-field-cooled ring No. 1 (open symbols) which was etched out from the disk No. 1. A magnetic field of 750 G was used to saturate the trapped magnetic field and the persistent current.

[Fig. 1(a)], show a very smooth pyramidlike shape. No surface steps which could suggest the influence of the Bean-Livingston surface barriers have been observed over the applied temperature range. The existence of the surface steps in the magnetic induction at the edges of a zero-field-cooled YBCO single crystal in the magneto-optically measured induction profiles (for the applied magnetic fields of 290–330 G and temperatures 55–60 K) have been interpreted by Dorosinskii, Nikitenko, and Polyanskii[12] as due to the Bean-Livingston surface barriers. The pyramidlike shape of the induction profiles generated by the thin-film disks [Fig. 1(a)] is observed at all applied temperatures (over a range of 64–84 K). These profiles do not provide any indication of a crossover between the partial and complete flux penetration into the disk. The partial-complete flux-penetration crossover can be seen in the temperature dependence of the profiles of the magnetic field trapped in the zero-field-cooled disk [Fig. 1(b)] when a constant external field is applied to the sample. It is interesting that the nonuniform flux trapping observed at temperatures corresponding to a partial flux-penetration regime transforms itself into the uniform one at higher temperatures when the whole sample is in the critical state (in the complete flux-penetration regime). By simply plotting the magnitude of the magnetic field trapped in the disk's center (which is measured after applying and subsequently removing a constant external field) versus temperature (Fig. 2), one can determine the crossover temperatures from the partial to complete flux penetration. This temperature is also given by the inflection point on the shielding field-temperature curve [Figs. 2(a)–2(c)]. The crossover temperature decreases with the increasing magnitude of the applied magnetic field [Fig. 2(d)]. All crossover temperatures indicate the maximum amount of the field $(B_z)_{\max}$ that can be trapped in the disk's center. This means that at temperatures above the crossover temperatures the full critical state is reached across the disk. In this regime, $B_z(T)_{\max}$ is proportional to temperature; $B_z(T) \propto (T - T_c)$. $B_z(T)_{\max}$ is also proportional to the minimum applied magnetic field B^* required for the complete flux penetration at a given temperature. This is not surprising since B^* equals $B_z \propto I_c$, the field shielded at the surface and in the center of the disk, when it just reached the full critical state. The proportionality of $B_z(T)_{\max}$ to $I_c(T)$ means that both must have the same temperature dependence. This was verified using a ring-shaped sample which was etched from disk No. 1. In the persistent current mode, the magnetic induction generated in the ring's center is due entirely to the current and it is directly proportional to the magnitude of the current. The measurements of the saturation value of the magnetic induction at various temperatures gave $I_c(T) \propto (T - T_c)$, the same temperature dependence as that for $B_z(T)_{\max}$ trapped in the disk's center (Fig. 4). $B_z(T)_{\max} \propto I_c(T)$ for the disk is also consistent with the calculation of the magnetic induction from the Biot-Savart law.[2,4,13,14]

The partial and complete flux-penetration regimes for the disk are characterized by different flux-relaxation phenomena. In the complete flux-penetration state, the normalized decay rate $S = (1/B_0)(dB/d \ln t)$ measured at various points across the disk fluctuates between 0.012 and 0.015 (with an average value of 0.0135). In the partial flux-penetration state S changes from a minimum value of 0.0045 at the disk's center up to a maximum equilibrium value of 0.012 at the disk's edge (Fig. 5). We have not observed a distinct influence of the Bean-Livingston surface effects on the magnetic relaxation across the sample. In the trapped field mode ($H_{\text{appl}}=0$), the Bean-Livingston model[15] assumes the flux lines near the surface experience an attractive image force to the surface, causing the energy per unit length to increase with a distance from the surface and in consequence faster magnetic relaxation at the surface in comparison to that in the bulk.

The magnitude of S measured in the complete flux-penetration state and that measured in the disk's center in the partial flux-penetration state is weakly temperature dependent [Figs. 5(c) and 5(d)] and independent of the magnitude of the trapped magnetic flux. S jumps to higher values above a temperature of 74 K which corresponds to a transition between incomplete and complete flux penetration after applying a magnetic field of 200 G. The weak temperature dependence of S in the disk's center for an incomplete penetration is surprising but it could mean that we record S in the complete flux penetration reduced by a constant amount of the flux-creep rate towards the center of the disk. The weak temperature dependence of S is also seen for the partial critical state in ring No. 1 [Fig. 7(a)]. The trapped flux in the ring [Fig. 7(b)] is a superposition of the self-field due to a persistent circulating current and the field of vortices trapped in the bulk of the ring. A persistent current can be induced in the

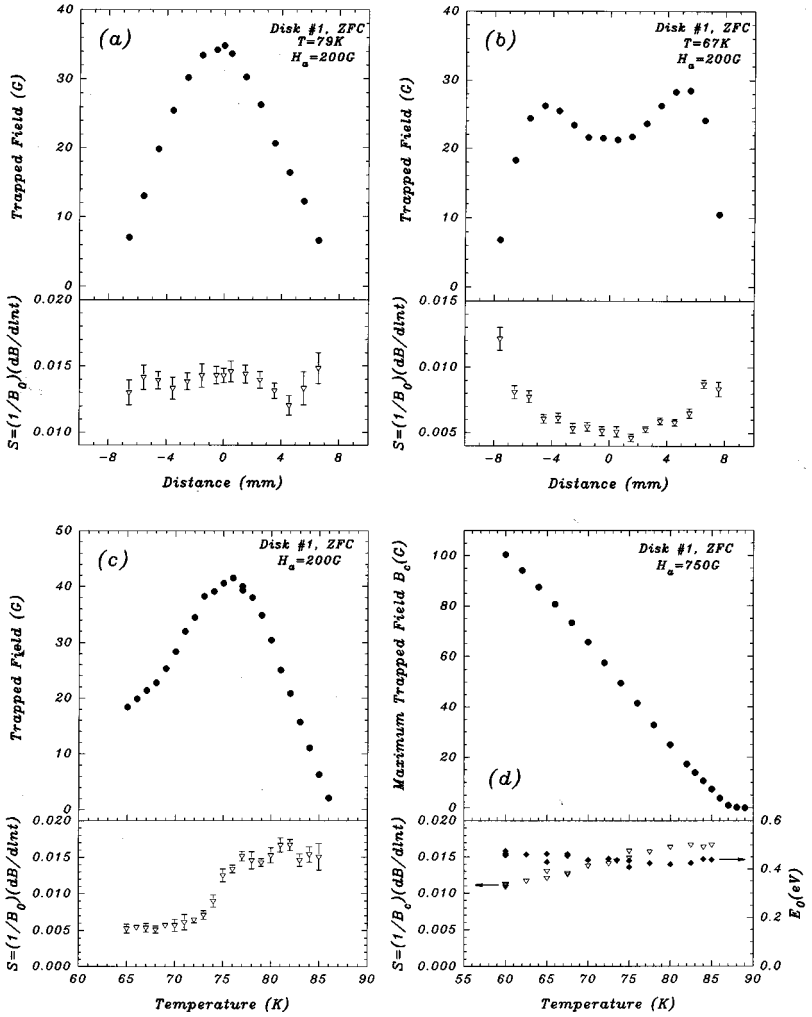

FIG. 5. (a) The upper part: The distributions of the trapped magnetic field measured across disk No. 1 at 79 K, which represent the case of the complete flux penetration after a field of 200 G was applied to the zero-field-cooled sample. The lower part: The corresponding distributions of the normalized decay rate $S=(1/B_0)dB/d\ln t$ for the motion of the trapped flux. (b) The distributions of the trapped field and the normalized decay rate S measured across disk No. 1 at 67 K, which represent the case of the incomplete flux penetration after a field of 200 G was applied to the zero-field-cooled sample. (c) Temperature dependence of the trapped field and the normalized decay rate S measured in the center of disk No. 1 when a field of 200 G was applied to the zero-field-cooled sample. (d) Temperature dependence of the maximum trapped field, the normalized decay rate S and the corresponding flux-pinning energy E_0 measured in the center of disk No. 1 when a saturating magnetic field of 750 G was applied to the zero-field-cooled sample.

ring when a magnetic flux is introduced into the ring's hole by applying and subsequently switching off the external magnetic field. During this process, the ring's bulk is fully penetrated by the magnetic flux, however, the ring is in the partial critical state as long as the magnitude of the circulating persistent current is below its critical value. For the ring, the superposition of both the vortex field and the persistent current's self-field produces smooth pyramid-shaped distributions of $B_z(r)$, the same for both the partial and complete critical states [see Fig. 7(b)], however, S exhibits a sharp jump to higher values at a temperature of 63.5 K which corresponds to a transition between the partial and the complete critical states after applying a magnetic field of 200 G. In the partial critical state, S has a value approximately two times less than the corresponding one for the disk. In the full critical state S matches the values obtained for the disk over the same temperature range, confirming independence of S on the sample geometry in the complete critical state regime. In the partial critical state regime, the behavior of $S(T)$ is similar for both the disk and the ring, however, the ring's geometry allows one to reach a full critical state at a lower temperature than the corresponding one for the disk. It appears that S in the partial critical state is governed by the effective gradient of $\partial B_z/\partial r$, however, we believe that the distributions of the critical currents or $B_r(r)$ in the disk and the ring could provide more definite explanation. The weak temperature dependence of S in the full critical state close to T_c for the disk and the ring [Fig. 5(d) and 7(a)] is consistent with data of Keller *et al.*[16] and Isaac *et al.*[17] on the c-axis melt-textured YBCO at remanence after application of saturating fields along the c axis, and with Malozemoff's and Fisher's model[18] of universality in the current decay and flux creep of YBCO. Close to T_c (over an applied temperature range of 60–85 K), the normalized decay rate from the maximum value of the trapped field $S=(1/B_c)(dB/d\ln t)=kT/E_0$ gives the energy barrier in the absence of flux creep E_0 independent of temperature, with an average value of 0.45 eV. This number is very close to that reported for the c-axis-oriented melt-textured YBCO.[16,17]

The measurement of the trapped field profiles at constant temperature for various stages of flux penetration into disk No. 2 confirmed that even in the early stages of flux penetration, the full critical state is reached at the disk's edge and it spreads steadily into the disk's center [Fig. 6(a)]. The full critical state is marked by the bell-shaped external envelope of fixed gradient $\partial B_z/\partial r$. This gradient decreases down to zero, when temperature of the disk is increased up to T_c [Fig. 6(b)]. The maximum trapped field $B_z(T)_{\max}$ is proportional to $I_c(T)$, however, the gradient $(\partial B_z/\partial r)(T)$ does not represent $J_c(T)$. According to calculations performed by Däumling and Larbalestier,[4] the magnitude of the trapped magnetic field in the disk's center plane ($z=0$) and in the disk's center

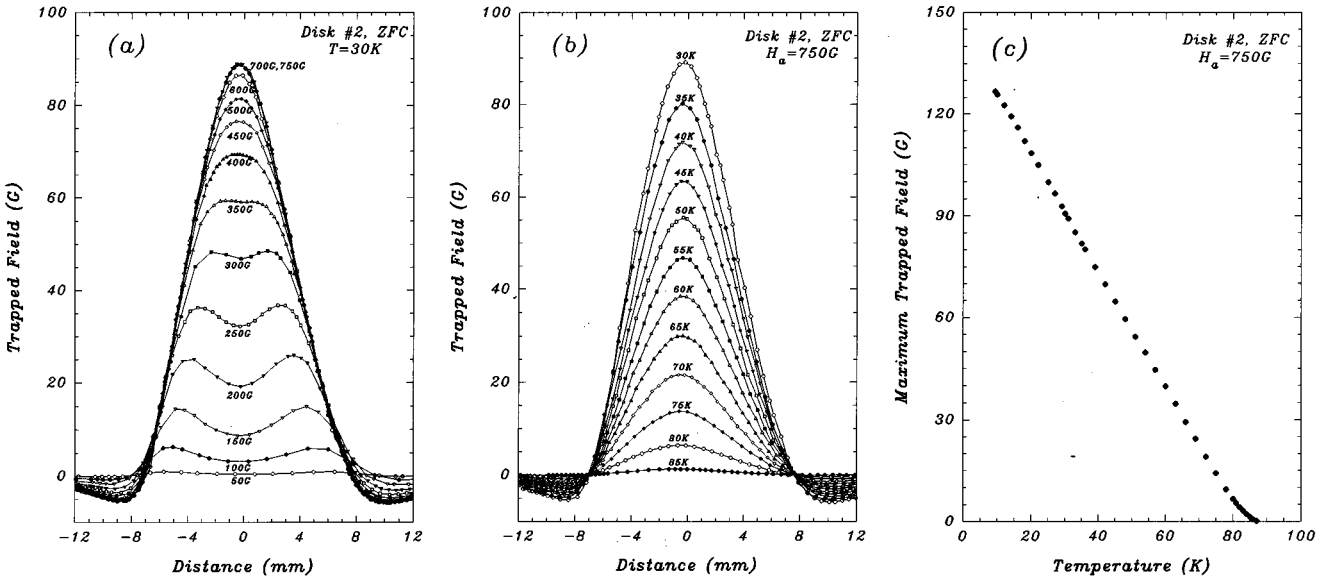

FIG. 6. (a) The distributions of the trapped field in disk No. 2 at 30 K, showing different stages of flux penetration after an increasing applied field (up to 750 G) was applied to the zero-field-cooled sample. Distances +7.5 and −7.5 mm mark the edges of the disk. (b) The distributions of the maximum trapped field in the zero-field-cooled disk No. 2 at various temperatures between 30 and 85 K. An applied field of 750 G was used to reach saturation at each temperature. (c) Temperature dependence of the maximum magnitude of the field trapped in the center of the zero-field-cooled disk No. 2 after applying an external field of 750 G.

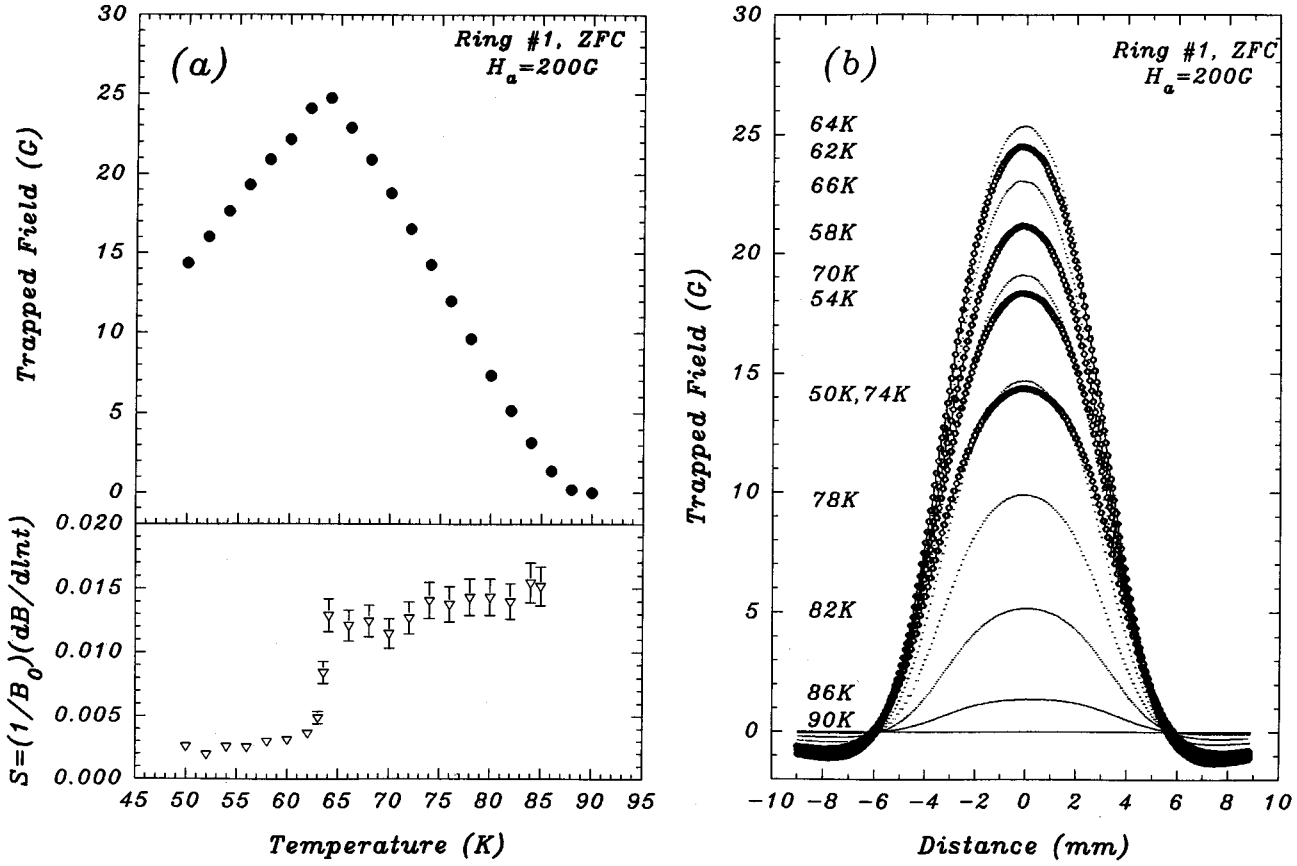

FIG. 7. (a) Temperature dependence of the trapped field and the normalized decay rate S measured in the center of ring No. 1 when a field of 200 G was applied to the zero-field-cooled sample. (b) The distributions of the trapped field in ring No. 1 at various temperatures between 50 and 86 K, after an external field of 200 G was applied to the zero-field-cooled sample. Distances +4.25, −4.25 mm and +2.50, −2.50 mm mark the outer and inner ring's edges, respectively.

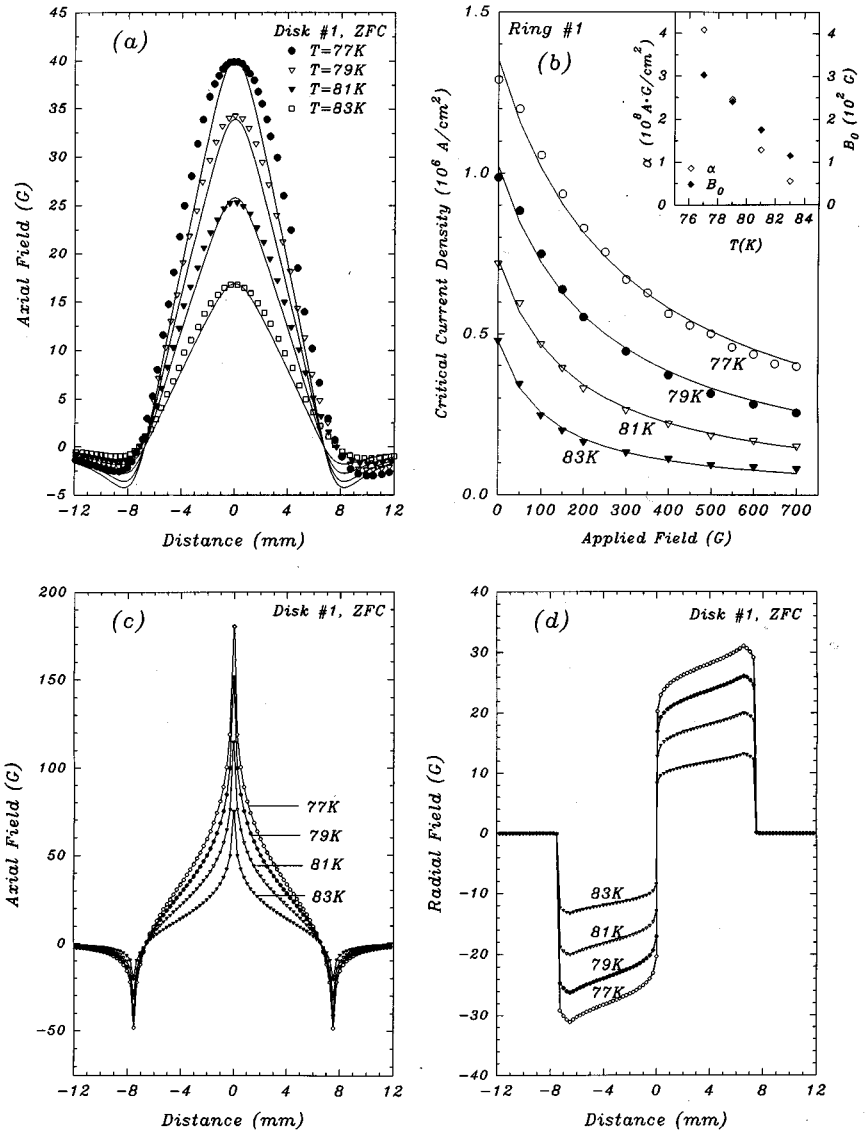

FIG. 8. (a) Symbols represent the profiles of the axial magnetic field trapped in the zero-field-cooled disk No. 1 (the measurement was done with a scanning Hall probe at a distance of 1.6 mm from the disk's surface) at temperatures of 77, 79, 81, and 83 K. A field of 200 G was used to saturate the trapped magnetic field. Solid lines represent the computer computations of the trapped field using the Biot-Savart equations and the Kim's relationships at temperatures of 77, 79, 81, and 83 K [see Fig. 8(b)]. Distances of +7.5 and −7.5 mm mark the disk's edges. (b) Symbols represent the magnetic-field dependence of the critical current density in the zero-field-cooled ring No. 1 at 77, 79, 81, and 83 K. Solid lines represent the Kim's relationships for $J_c(B)=\alpha/(B+B_0)$ with constants $\alpha(T)$ and $B_0(T)$ given in the inset. (c) Computer simulations of the profiles of the axial component of the field trapped in the zero-field-cooled disk No. 1 at 77, 79, 81, and 83 K. $B_z(r)$ was calculated on the disk's surface using the Biot-Savart equations and the Kim's relationships shown in (b). Distances +7.5 and −7.5 mm mark the disk's edges. (d) Computer simulations of the profiles of the radial component of the field trapped in the zero-field-cooled disk No. 1 at 77, 79, 81, and 83 K. $B_r(r)$ was calculated on the disk's surface using the Biot-Savart equations and the Kim's relationships shown in (b). Distances +7.5 and −7.5 mm mark the disk's edges. Note the change in the radial field $B_r(r)$ over a distance $0<r<a$. A decrease in the radial field from a maximum value is about 3.5% per millimeter for all temperatures of the measurement.

$(r=0)$ is of order $J_c d$. For disk No. 1 the magnitude of J_c at 77 K is 1.30×10^6 A/cm^2 (obtained from the measurement of the saturation value of the magnetic induction in the center of ring No. 1, which is directly proportional to the critical current). The maximum trapped magnetic field at $z=0$ and $r=0$ should therefore be equal to about 800 G at 77 K. The experiment gives the maximum trapped field of about 40 G at $z=1.6$ mm and $r=0$ [Fig. 1(b)], which was obtained by applying a minimum external magnetic field of 200 G. It means that Däumling and Larbalestier formula overestimates the magnitude of the trapped field since it cannot be higher than that of the applied field. The reason for this is that the $J_c d$ formula is valid for magnetic-field independent J_c. The real J_c could be much smaller because of the presence of the local self-fields generated by concentric loops of current flowing in the disk.[5] The self-fields may well exceed 200 G.

The question is what is the relationship between the profile of the trapped axial magnetic field as seen by a scanning Hall probe at a distance of 1.6 mm above the thin-film disk to that observed in YBCO disk-shaped thin films by means of magneto-optical methods at a distance of 0.2 μm above the surface of the film (Ref. 3).

We performed computer simulations of $B_z(r,z)$ and $B_r(r,z)$ in the zero-field-cooled disk No. 1 at temperatures of 77, 79, 81, and 83 K, using the computation methods described in Refs. 4, 5, and 13. The disk was divided into 150 000 ring segments. The axial field $B_z(r,z)$ and the radial field $B_r(r,z)$ generated by the current in each ring segment was calculated from the Biot-Savart equation.[19] The total axial field above the sample was calculated by summing up the contributions from the individual current loops. The influence of the self-fields was incorporated into the calculations using the iteration procedure and taking a field dependent $J_c=\alpha/(B+B_0)$ according to Kim's relationship,[20] with the constants α and B_0 determined at 77, 79, 81, and 83 K from the measurement of the magnetic-field dependence of the critical current density in ring No. 1 [Fig. 8(b)]. The results for B_z $(r,z=1.6$ mm) are shown in Fig. 8(a) together with the experimental data for disk No. 1 at 77, 79, 81, and 83 K measured by a scanning Hall probe. The results for B_z $(r,z=0.25$ μm) on the disk's surface are given in Fig. 8(c). The shape of the profile at $z=0.25$ μm resembles those observed on the surface of thin-film disks with a magneto-optical method.[2,3] The gradient $\partial B_z/\partial r$ at $r=a/2$ and on the

disk's surface is about a factor of 2 larger than the corresponding one measured by a Hall probe at a distance of 1.6 mm from the disk's surface. At 77 K, the axial field gradient on the disk's surface at $r=a/2$ is equivalent to the current density $(1/\mu_0)\partial B_z/\partial r=0.88\times10^2$ A/cm^2. The ratio of J_c (obtained for the ring No. 1 at 77 K) to the current density produced by the axial field gradient on the disk's surface is $J_c/[(1/\mu_0)\partial B_z/\partial r]=(1.30\times10^6$ A/cm$^2)/(0.88\times10^2$ A/cm$^2)$ $=1.5\times10^4$. This is equal to the aspect ratio $a/d=$radius/thickness$=1.5\times10^4$, in agreement with the estimation of the ratio $(\partial B_r/\partial z)/(\partial B_z/\partial r)\simeq a/d$ in Ref. 3.

The results for B_r $(r,z=0.25$ μm) on the disk's surface at temperatures of 77, 79, 81, and 83 K are shown in Fig. 8(d). $J_c(r)=2(1/\mu_0)B_r/d$ represents the distribution of the critical currents. The maximum critical current density occurs at the disk's edge at $r=a$. $J_c(r)$ decreases with r at a rate of about 3.5% per millimeter. This rate is independent of temperature. Regarding the behavior of $J_c(r)$, it is interesting to compare the results of the measurements of the flux and current distributions in a disk-shaped YBCO thin film with those obtained for a square-shaped YBCO thin film (Refs. 8, 9). In the work done by Xing *et al.* and Grant *et al.* (Refs. 8, 9), a scanning Hall probe was applied in order to determine an x-y distribution of the axial magnetic field B_z at a temperature of 77 K, and at a distance of 0.25 mm from the sample surface. They constructed a surface map of the saturation magnetization of the YBCO film, which was calculated from the measured $B_z(x,y)$ using the inverse matrix method. The scans of the critical current densities $J_c(x)$ and $J_c(y)$ across the sample were obtained by computing the spatial derivatives of the magnetization. The magnitude of $J_c(x)$ and $J_c(y)$ has a maximum near the sample edges. $J_c(x)$ and $J_c(y)$ decrease from a value of $\sim3\times10^6$ A/cm^2 at the edge with decreasing x and y at a rate of approximately 14% per millimeter, a factor of 4 larger than the corresponding rate for disk-shaped YBCO thin film. The temperature dependence of $B_r(r)$ in Fig. 8(d) shows that the gradient in $J_c(r)$ is independent of the magnitude of J_c. The increase in the gradient of $J_c(r)$ must, therefore, be caused by the sample square geometry. Recent work on the current and field pattern in rectangular and inhomogeneous superconductors by Schuster *et al.*[21] implies that in square-shaped samples a strong concentration of electric field can occur along the lines where J_c changes abruptly. This means a high flux-flow rate and dissipation of energy.

V. SUMMARY

We investigated the temperature dependence of the penetration process of the magnetic flux into disk-shaped YBCO thin films, especially the transition between the partial and complete flux-penetration states. The complete flux-penetration state is characterized by the normalized logarithmic decay rates constant across the disk $(0.012<S<0.015)$. S in the partial flux penetration state has a minimum in the disk's center $(S\simeq0.005)$ and a maximum $(S\simeq0.012)$ at the disk's edges. The temperature dependence of the magnetic induction at the transition is governed by the temperature dependence of the critical current. The maximum field trapped in the disk's center and the self-field of the critical current flowing in the ring (which was etched out from the disk) have the same temperature dependence. This confirms that the trapped- or shielding-field profiles above the thin-film disk can be simulated by summing up the self-fields of a large number of concentric current loops. The experiment also confirms that the critical current density $J_c\simeq(1/\mu_0)\partial B_r/\partial z$ exceeds the current density produced by the axial field $(1/\mu_0)\partial B_z/\partial r$ by the factor of radius/thickness. We did not observe any flux-penetration effects at the disk's edges, which would suggest the presence of the Bean-Livingston surface barriers in contradiction to recently reported experiments on YBCO single crystals[12] for the similar range of applied magnetic field. We believe that the sample's nonuniformities at the sample's edges may produce Bean-Livingston-like effects.

ACKNOWLEDGMENTS

We are pleased to acknowledge useful discussions with J. R. Clem. This work was supported by a grant from the Natural Sciences and Engineering Research Council of Canada (NSERC).

*Current address: The University of Northern British Columbia, Prince George, BC, Canada, V2N 4Z9.

[1] Y. Yokoyama, Y. Hasumi, H. Obara, Y. Suzuki, T. Katayama, S. Gotoh, and N. Koshizuka, Jpn. J. Appl. Phys. **30**, L714 (1991).
[2] A. Forkl, Phys. Scr. T **49**, 148 (1993).
[3] H. Theuss, A. Forkl, and H. Kronmüller, Physica C **190**, 345 (1992).
[4] M. Däumling and D. C. Larbalestier, Phys. Rev. B **40**, 9350 (1989).
[5] L. W. Conner and A. P. Malozemoff, Phys. Rev. B **43**, 402 (1991).
[6] E. H. Brandt, Physica C **235–240**, 2939 (1994).
[7] M. A-K. Mohamed, J. Jung, and J. P. Franck, Phys. Rev. B **39**, 9614 (1989).
[8] W. Xing, B. Heinrich, H. Zhou, A. A. Fife, and A. R. Cragg, J. Appl. Phys. **76**, 4244 (1994).
[9] P. D. Grant, M. W. Denhoff, W. Xing, P. Brown, S. Govorkov, J. C. Irwin, B. Heinrich, H. Zhou, A. A. Fife, and A. R. Cragg, Physica C **229**, 289 (1994).
[10] J. Talvacchio, M. G. Forrester, J. R. Gavaler, and T. T. Braggins, in *Science and Technology of Thin Film Superconductors II*, edited by R. McConnell and S. A. Wolf (Plenum, New York, 1990), pp. 57–66.
[11] J. Jung, I. Isaac, and M. A-K. Mohamed, Phys. Rev. B **48**, 7526 (1993).
[12] L. A. Dorosinskii, V. I. Nikitenko, and A. A. Polyanskii, Phys. Rev. B **50**, 501 (1994).
[13] D. J. Frankel, J. Appl. Phys. **50**, 5402 (1979).
[14] J. D. Jackson, *Classical Electrodynamics* (Wiley, New York, 1962).
[15] C. P. Bean and J. D. Livingston, Phys. Rev. Lett. **12**, 14 (1964).
[16] C. Keller, H. Küpfer, R. Meier-Hirmer, U. Welch, V. Selvamanickam, and K. Salama, Cryogenics **30**, 410 (1990).
[17] I. Isaac, J. Jung, M. Murakami, S. Tanaka, M. A-K. Mohamed,

and L. Friedrich, Phys. Rev. B **51**, 11 806 (1995).
[18] A. P. Malozemoff and M. P. A. Fisher, Phys. Rev. B **42**, 6784 (1990).
[19] W. R. Smythe, *Static and Dynamic Electricity* (McGraw-Hill, New York, 1939), p. 266.
[20] Y. B. Kim, C. F. Hempstead, and A. R. Strnad, Rev. Mod. Phys. **36**, 43 (1964).
[21] T. Schuster, H. Kuhn, E. H. Brandt, M. V. Indenbom, M. Kläser, G. Müller-Vogt, H. Kronmüller, and A. Forkl, Phys. Rev. B **52**, 10 375 (1995).